Pembrolizumab in Combination with the Oncolytic Virus Pelareorep and Chemotherapy in Patients with Advanced Pancreatic Adenocarcinoma: A Phase Ib Study

Devalingam Mahalingam[1,2], Grey A. Wilkinson[3], Kevin H. Eng[4], Paul Fields[5], Patrick Raber[5], Jennifer L. Moseley[2], Karol Cheetham[3], Matt Coffey[3], Gerard Nuovo[6], Pawel Kalinski[4], Bin Zhang[1], Sukeshi Patel Arora[2], and Christos Fountzilas[4]

ABSTRACT

Purpose: Pelareorep is an intravenously delivered oncolytic reovirus that can induce a T-cell–inflamed phenotype in pancreatic ductal adenocarcinoma (PDAC). Tumor tissues from patients treated with pelareorep have shown reovirus replication, T-cell infiltration, and upregulation of PD-L1. We hypothesized that pelareorep in combination with pembrolizumab and chemotherapy in patients with PDAC would be safe and effective.

Patients and Methods: A phase Ib single-arm study enrolled patients with PDAC who progressed after first-line treatment. Patients received pelareorep, pembrolizumab, and either 5-fluorouracil, gemcitabine, or irinotecan until disease progression or unacceptable toxicity. Study objectives included safety and dose-limiting toxicities, tumor response, evaluation for reovirus replication, and immune analysis in peripheral blood and tumor biopsies.

Results: Eleven patients were enrolled. Disease control was achieved in three of the 10 efficacy-evaluable patients. One patient achieved partial response for 17.4 months. Two additional patients achieved stable disease, lasting 9 and 4 months, respectively. Treatment was well tolerated, with mostly grade 1 or 2 treatment-related adverse events, including flu-like symptoms. Viral replication was observed in on-treatment tumor biopsies. T-cell receptor sequencing from peripheral blood revealed the creation of new T-cell clones during treatment. High peripheral clonality and changes in the expression of immune genes were observed in patients with clinical benefit.

Conclusions: Pelareorep and pembrolizumab added to chemotherapy did not add significant toxicity and showed encouraging efficacy. Further evaluation of pelareorep and anti–PD-1 therapy is ongoing in follow-up studies. This research highlights the potential utility of several pretreatment and on-treatment biomarkers for pelareorep therapy warranting further investigation.

Introduction

Pancreatic ductal adenocarcinoma (PDAC) is the third-leading cause of cancer-related death in the United States (1) with a 5-year overall survival (OS) of only 5% (2). Most patients present with advanced disease (3) and, despite recent advances in management (4, 5), almost all patients will eventually succumb to their disease. Therefore, new treatment options are urgently needed. One novel option is oncolytic virus immunotherapy, which uses wild-type or genetically modified viruses to selectively kill tumor cells and promote tumor-directed innate and adaptive immune responses (6). The oncolytic reovirus pelareorep is a proprietary isolate of the reovirus type III Dearing strain. Selective viral replication and lysis in cancer cells is influenced by multiple factors, including upstream and downstream mediators of RAS and PKR signaling pathways (6). Preclinical and clinical studies have revealed that reovirus replication and lysis is enhanced by combination treatments with several chemotherapies, including taxanes, gemcitabine, and irinotecan (7–9).

Pelareorep was safely combined with gemcitabine in a phase I study in patients with advanced cancer (8). Overall, the combination was assessed as safe, and the most common toxicities were manageable "flu-like" and gastrointestinal symptoms (8). The combination displayed clinical activity in this highly pretreated patient population. In a follow-up phase II, single-arm, open-label study pelareorep was administered in combination with gemcitabine in 34 chemotherapy-naïve patients with advanced PDAC (9). Treatment was well tolerated with manageable nonhematologic toxicities (9). One patient attained a partial response (PR), while 23 patients had stable disease (SD) as best response. The median OS was 10.2 months, with a 1- and 2-year survival rate of 45% and 24%, respectively. Despite modest advances in pelareorep plus chemotherapy combinations, the immunogenic properties of pelareorep have spurred investigations that examine combinations with immune checkpoint blockade inhibitors (ICI; refs. 10–12).

Antiviral immune responses help trigger antitumor immunity (13). Antiviral immune responses to pelareorep are mediated by the detection of dsRNA (via Toll-like receptors and pattern recognition receptors), which stimulate the secretion of IFNs, inflammatory cytokines, and upregulate innate immune response genes such as PD-L1 and antigen processing genes such as TAP1/2 and HLAs (14–16). Moreover, innate activation leads to T- and natural killer (NK) cell infiltration into the tumor microenvironment (TME), priming the TME, and serving as an adjunct to ICIs (13, 17–20). On-treatment primary pancreatic tumor biopsies

[1]Robert H. Lurie Comprehensive Cancer Center, Northwestern University, Chicago, Illinois. [2]Mays Cancer Center, University of Texas Health San Antonio, San Antonio, Texas. [3]Oncolytics Biotech Inc, Calgary, Alberta, Canada. [4]Roswell Park Comprehensive Cancer Center, Buffalo, New York. [5]Adaptive Biotechnologies, Seattle, Washington. [6]Ohio State University Arthur G. James Cancer Hospital and Richard J. Solove Research Institute, Columbus, Ohio.

Note: Supplementary data for this article are available at Clinical Cancer Research Online (http://clincancerres.aacrjournals.org/).

Corresponding Author: Devalingam Mahalingam, Robert H. Lurie Comprehensive Cancer Center, Northwestern University, 233 E Superior, Chicago, IL 60611. Phone: 210-413-1723; E-mail: Mahalingam@northwestern.edu

Clin Cancer Res 2020;26:71–81

doi: 10.1158/1078-0432.CCR-19-2078

Translational Relevance

This study demonstrates that combination therapy with pelareorep, an intravenously delivered oncolytic virus, in combination with pembrolizumab and chemotherapy is safe and well tolerated in patients with pancreatic ductal adenocarcinoma. Efficacy results are encouraging in this difficult to treat patient population. Biomarker analysis reveals striking changes to the peripheral T-cell repertoire, with early and durable clonal expansion being associated with longer overall survival. Changes in peripheral T-cell clonality should be examined as a dynamic predictive biomarker in future studies with oncolytic viruses. Upregulation of CCR5 pathway and CCR5 ligands should also be evaluated as a potential negative predictive biomarker.

in the phase II study of pelareorep in combination with gemcitabine showed viral replication and upregulation of PD-L1 and apoptosis in cancer cells (9).

We hypothesized that, as PD-L1 is upregulated in nonneoplastic tissue after chronic viral infection to minimize immune system-induced damage (21), PD-L1 upregulation in PDAC after oncolytic virotherapy can be an inducible defense mechanism that can be exploited for ICI therapy. Furthermore, we hypothesized that active viral replication in PDAC can promote a favorable antitumor immune response and "prime" PDAC, a notoriously "immune-cold" tumor, for ICI therapy. To test our hypothesis, we designed a phase Ib trial to evaluate the efficacy and safety of combination therapy with intravenously administered pelareorep, chemotherapy, and pembrolizumab in patients with advanced PDAC who had received first-line therapy (NCT02620423). This study, to our knowledge, is the first to combine an ICI with a systemically delivered oncolytic virotherapy in PDAC. We also performed an in-depth evaluation of the effects of pelareorep on systemic immunity with sequential pembrolizumab administration.

Patients and Methods

Trial patients

Eleven patients ($\geq$18 years of age) with an Eastern Cooperative Oncology Group (ECOG) performance status of 0 to 2 and advanced (unresectable or metastatic) histologically confirmed PDAC who progressed after (or did not tolerate) first-line treatment were recruited into this trial. Eligible patients had measurable disease by the RECIST version 1.1 (22), adequate bone marrow, liver, and kidney function at baseline as well as no evidence of endocrinopathy or proteinuria. Key exclusion criteria included active autoimmune disease, any use of immunosuppressive therapy, known human immunodeficiency virus (HIV) infection, active hepatitis B or C, clinically significant congestive heart failure (New York Heart Association Class III or IV) including preexisting arrhythmia, uncontrolled angina pectoris, recent myocardial infarction, and grade 2 or higher compromised left ventricular ejection fraction.

All patients gave their written informed consent before their enrollment to the study. The protocol was approved by the ethics and scientific committees at the University of Texas Health Science Center at San Antonio on December 9, 2015. This study was conducted according to the Helsinki declaration and the guidelines on good clinical practice.

Trial design, treatment, and procedures

This was a single-arm, open-label, nonrandomized phase Ib trial (**Fig. 1A**). Patients were treated on a 21-day cycle with one of three chemotherapy backbone regimens based on physician preference: (i) gemcitabine 1,000 mg/m^2 intravenously on day 1, (ii) irinotecan 125 mg/m^2 i.v. on day 1, or (iii) leucovorin 200 mg/m^2 and 5-fluorouracil (5-FU) 200 mg/m^2 i.v. bolus on day 1, followed by 5-FU 1,200 mg/m^2 continuous intravenous infusion over 22 hours on day 1. The choice for chemotherapy backbone was based on the patient's prior chemotherapy exposure and investigator preference.

Pelareorep was administered at 4.5×10^{10} $TCID_{50}$ (50% tissue culture infective dose) intravenously on days 1 and 2 after chemotherapy infusion. Pembrolizumab was administered at 2 mg/kg i.v. on day 8 (dosing based on the package insert at the time of the study design).

After three patients were initially enrolled with no dose-limiting toxicity (DLT), the study was expanded by the addition of eight patients. Patients were treated until disease progression or intolerable toxicity (that did not respond to either supportive care or dose reduction).

Chemotherapy and pelareorep dose modifications were allowed (Supplementary Table S1); the dose of chemotherapy or pelareorep was decreased by one dose level for ANC $< 0.5 \times 10^9$/L lasting for >7 days, ANC $< 0.5 \times 10^9$/L with sepsis, platelet count $<25 \times 10^9$/L, grade 2 neurotoxicity or cardiotoxicity. The dose was also decreased for any other drug-related nonhematologic grade 3 or 4 toxicity (with exception of flu-like symptoms, nausea, vomiting, and diarrhea in the absence of appropriate prophylactic or therapeutic measures) or inability to tolerate one course of therapy due to toxicity. No dose modifications were allowed for pembrolizumab.

Safety assessments were performed on days 1, 8, and 15 of cycle 1, and days 1 and 8 of subsequent cycles. Adverse events were characterized using the Common Terminology Criteria for Adverse Events (CTCAE), version 4. Disease assessment with cross-sectional imaging (CT or MRI) was performed at baseline and every three cycles. Tumor assessments were performed using the immune-related response criteria (23) and RECIST 1.1. Tumor biopsies were performed at baseline, if archival tissue was not available, as well as once between cycle 2 day 15 and cycle 3 day 1. Peripheral blood, including peripheral blood mononuclear cells (PBMC), was collected on cycle 1 day 1 (pretreatment), cycle 1 day 8 (prior to pembrolizumab), and cycle 2 day 1 (pretreatment) for correlative studies.

Trial objectives

The primary objective was to determine the safety and DLTs of pelareorep and chemotherapy in combination with pembrolizumab. Secondary objectives were: (i) to determine the overall response rate (ORR) and progression-free survival (PFS) by immune-related response criteria (23), as well as OS; and (ii) to determine the effects of pelareorep and pembrolizumab when administered in combination as determined by analysis of pre- and posttreatment biopsies and blood-based immune markers.

Histology

An antibody against reovirus capsid protein was provided by Dr. Matt Coffey (Oncolytics Biotech Inc.). Antibodies against PD-L1, IDO-1, caspase-3, and CD8 were obtained from Abcam. Each was detected using the Leica Bond Max's DAB Refine Kit with an anti-rabbit-HRP provided by Enzo Life Sciences as previously published (24). The viral RNA *in situ* hybridization protocol has been described previously (24). The cell counts for CD8, PD-L1, caspase-3, and IDO1 were compiled by counting the number of positive cells/in

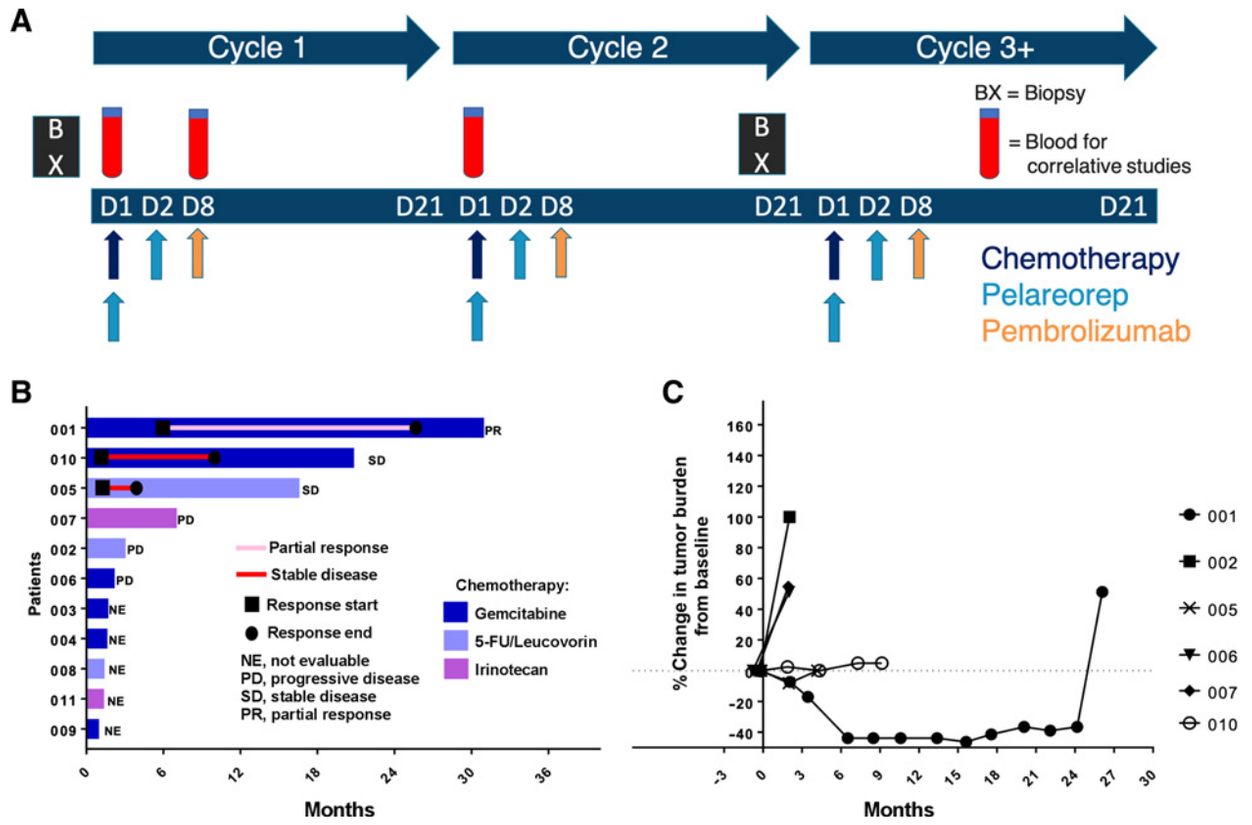

Figure 1.

Second-line treatment of pancreatic cancer with pelareorep, pembrolizumab, and chemotherapy results in disease control in disease control in three of the 10 efficacy-evaluable patients. **A,** Overview of study schedule indicating scheduled tumor biopsies (BX) and blood draw for correlative studies (CS). **B,** Swimmers plot of survival time of patients on study. **C,** Spider plot of tumor response based on the sum maximum diameter changes in target lesions.

multiple 200× fields. At least 3,000 cells were counted and mean (and SD) was derived and analyzed with the InStat Statistical Analysis Software (version 3.36).

TCR immunosequencing

Immunosequencing of the CDR3 regions of human T-cell receptor-β (TCRβ) chains was performed using the ImmunoSEQ Assay developed by Adaptive Biotechnologies. DNA for this assay was isolated from PBMCs collected at cycle 1 day 1 (C1D1), C1D8, and C2D1. As previously described, TCRβ CDR3 regions were amplified by a multiplex, bias-controlled PCR with primers targeting the V and J genes of T cells as well as primers targeting housekeeping genes to quantitate the total nucleated cells in each sample (25). PCR products were sequenced on an Illumina NextSeq.

T-cell repertoire metrics include Simpson clonality, which is calculated as follows:

$$\text{Simpson clonality} = \sqrt{\sum p_i^2}$$

where p_i is the proportional abundance of clone i for all productive sequences. Diversity is determined as the number of unique rearrangements given a set number of T cells (2581 T cells in this case). Differential abundance was performed as described previously (26); briefly for each rearrangement, a *P* value was calculated by a binomial test based on the distribution of counts in each sample. A Benjamini–Hochberg multiple hypothesis was then performed on all rearrangements with a cumulative count of at least 5 in the two samples, and tests with an alpha value of less than 0.01 were assigned as differential.

PMBC gene expression profiling

RNA was extracted from PBMCs. The NanoString nCounter PanCancer Immune Profiling panel (NanoString Technologies) was used to characterize immune gene expression. Analysis was performed in nCounter Software 3. The software first identifies and checks standard QC controls such as imaging, binding density, and positive controls to ensure the samples were read and reported properly. The normalization was performed with positive controls as well as housekeeping gene normalization. The positive control normalization normalizes all platform-associated sources of variation. Reference (housekeeping) gene normalization was also performed to adjust counts of all probes relative to a probe set that is not expected to vary between samples.

Cytokine analysis

Serum was isolated from whole blood obtained on C1D1, C1D8, and C2D1. Forty-one cytokines (Eotaxin, GM-CSF, GROα, IFNα, IFNγ, IFNβ, IL1β, IL1α, IL1RA, IL2, IL4, IL5, IL6, IL7, IL8, IL9, IL10, IL12 p70, IL13, IL15, IL17A, IL18, IL21, IL22, IL23, IL27, IL31, MCP-1, MIP-1α, MIP-1β, RANTES, SDF1α, TNFα, TNFβ, IP-10/CXC10, MIG/CXCL9, ITAC/CXCL11, MDC/CCL22, CCL17/TARC,

CSF-1/M-CSF, VEGF-A) were measured in serum samples using the Luminex assay (HCYTOMAG-60K, HCYTOMAG-60K-17, HCYTOMAG-60K-01, HCYP2MAG-62K-04, HCYP3MAG-63K-03, HTH17MAG-14K-03, HCYP4MAG-64K-01, HIL18MAG-66K, EMD Millipore). IL18 was analyzed by combining HIL18-MAG-66K with HTH17MAG-14K according to the manufacturer's instructions. The dilution for RANTES was 1:100 in Assay Buffer, and that for IFNβ was 1:4, per the manufacturer's instructions. All assay runs were set up according to the manufacturer's instructions. The Luminex 100/200 instrument was set up to count at least 50 beads per analyte for all analytes.

Statistical analysis

This single-arm phase Ib study evaluated the combination of pelareorep, chemotherapy, and pembrolizumab. The study is descriptive in nature with the goal to define DLT, if any, and to recommend a dose for further studies. Statistical methods for gene expression profiling include standard upper quartile normalization of the targeted panel and analysis by linear models (R/Limma) incorporating patient and time point effects (27). FDR values were calculated by Benjamini and Hochberg's method (28). Throughout, *P* values are reported as unadjusted for multiple comparisons unless otherwise specified. All statistical tests for TCR immunosequencing were performed in R. For analysis of clonality, diversity and T-cell fraction over time as linear mixed model was performed. For PFS and OS, a Cox regression was performed. For comparisons between groups, a Wilcoxon rank-sum test was performed.

Results

Patients

A total of 11 patients were enrolled from January to August 2016. Overall, the median age was 64 years (range, 50–84) with 45% of patients ≥65 years of age (Supplementary Table S2). Most patients were female (73%), Caucasian (100%), and non-Hispanic (64%). All patients had an ECOG performance score of 0 (55%) or 1 (45%). Median CA 19.9 at baseline was 49 (range, 32–404). All patients received prior systemic chemotherapy. Four patients had a previous surgical resection, Whipple procedure, or total pancreatectomy. Patients were treated with pelareorep, pembrolizumab, and either gemcitabine ($n = 6$), LV/5-FU ($n = 3$), or irinotecan ($n = 2$).

Table 1. Treatment-related adverse events occurring at any grade in ≥10% of patients or ≥grade 3 in any patient.

Preferred term	Any grade	Grade 1/2	Grade 3	Grade 4
Any event, *n* (%)	10 (90.9)	10 (90.9)	1 (9.1)	1 (9.1)
Fever	9 (81.8)	8 (72.7)	1 (9.1)	0
Chills	6 (54.5)	5 (45.5)	1 (9.1)	0
Fatigue	3 (27.3)	3 (27.3)	0	0
Headaches	3 (27.3)	3 (27.3)	0	0
Anemia	2 (18.2)	2 (18.2)	0	0
Emesis	2 (18.2)	2 (18.2)	0	0
Flu-like symptoms	2 (18.2)	2 (18.2)	0	0
Hypotension	2 (18.2)	2 (18.2)	0	0
Nausea	2 (18.2)	2 (18.2)	0	0
Myalgias	1 (9.1)	1 (9.1)	1 (9.1)	0
Neutropenia	2 (18.2)	2 (18.2)	0	1 (9.1)
Leukopenia	1 (9.1)	0	0	1 (9.1)

Note: Toxicities are reported as per the Common Terminology Criteria for Adverse Events (CTCAE), version 4.

Safety

The median number of treatment cycles for all patients was three (range, 1–35). Treatment was well tolerated with manageable toxicities. Treatment-related adverse events (TRAE) occurring at any grade in ≥10% of patients or ≥grade 3 in any patient are presented in **Table 1**. TRAEs are defined as adverse events attributed to, or likely attributed to, any of the study drugs. The most common grade 1 or 2 TRAEs included fever (73%), chills (46%), fatigue (27%), headache (27%), anemia (18%), emesis (18%), flu-like symptoms (18%), hypotension (18%), nausea (18%), neutropenia (18%). One patient (gemcitabine arm) experienced transient grade 2 increased transaminases on two occasions. Grade 3 or 4 TRAEs were reported in two patients (18%) with one occurrence of neutropenia and leukopenia and one occurrence of myalgias, fever, and chills.

Antitumor activity – clinical efficacy

Ten of 11 patients were evaluable for efficacy, one patient achieved a PR 6.5 months after the start of therapy that lasted 17.4 months, two patients achieved SD 2 months after the start of therapy lasting 9.1 and 4.1 months, respectively, and three patients had progressive disease as the best response (**Fig. 1B**). No complete responses (CRs) were observed. Five patients were treated for less than three cycles secondary to clinical disease progression ($n = 4$) and toxicity/withdrawal of consent ($n = 1$) and were not evaluable for radiographic response assessment. Overall, the response rate and disease control rates were 9% and 27%, respectively. All patients died from their disease.

For all evaluable patients on study, the percentage change in response and duration of response is outlined in the spider plot (**Fig. 1C**). The median PFS was 2.0 months [95% confidence interval (CI), 0–6.8 months]. The median OS was 3.1 months (95% CI, 0–8.7 months), with a 1-year and 2-year survival of 35% and 23%, respectively.

Antitumor activity - intravenously delivered pelareorep replicates in tumor tissue

To examine whether pelareorep replicates in tumor tissue and promotes immunologic changes in the TME, we examined on-treatment biopsies collected at the end of cycle 2 but prior to the start of cycle 3. Paired tumor biopsies were collected from seven of the 11 patients, of which one set of collected samples was not suitable for analysis. An examination of reoviral dsRNA revealed that pelareorep replicates at high levels in the majority of tumor tissue, 54.9% to 78.4% (**Table 2**), with representative images from patient No. 002 presented in **Fig. 2A**. We also examined reoviral capsid protein to examine the extent of virus-induced cell lysis, revealing significantly lower levels of viral mediated lysis in tumor cells 0.5% to 4.3% (**Fig. 2B**), along with reoviral dsRNA co-localization analysis (**Fig. 2C**). However, cell lysis may not be necessary to mediate immunological changes in the TME given that dsRNA is a known immune adjuvant detected by pattern recognition receptors that promote interferon signaling (29).

To examine broad changes in the innate and adaptive immune response to treatment, we examined changes in PD-L1 and IDO1 expression as well as $CD8^+$ T-cell infiltration pre- and posttreatment (**Table 2**) with representative images from patient No. 002 presented in **Fig. 2D–F′**). Increases in the number of $CD8^+$ T cells were observed in all paired biopsies and were statistically significant in patients No. 002 and No. 004, while statistically significant increases in the expression of innate response genes PD-L1 and IDO1 were observed in patients No. 006 and No. 007, but not patient No. 004 and No. 002 (**Fig. 2E, 2E′**). IHC for the apoptosis marker, caspase-3, revealed and trended toward an increase in apoptosis in the on-treatment biopsies,

Table 2. Pre- and posttreatment histology analysis.

Patient number	Time point	Viral RNA[a] (SD)	Viral protein[a] (SD)	Caspase-3[a] (SD)	CD8[a] (SD)	PD-L1[b] (SD)	IDO 1[a] (SD)
002	Pre	0	0	6.1 (2.8)	16.9 (6.6)	31.3 (6.6)	37.5 (10.9)
	Post	65.7% (8.3)	4.3% (3.1)	11.1 (5.5)	37.0 (11.9)	25.6 (9.6)	27.7 (13.9)
004	Pre	0	0	—[c]	61.1 (13.3)	43.1 (7.9)	—[c]
	Post	54.9% (7.9)	2.3% (0.9)	11.2 (4.4)	153.9 (11.3)	42.9 (8.8)	13.9 (3.9)
005	Pre	0	0	—[c]	11.1 (4.4)	24.5 (4.4)	—[c]
	Post	—[c]	—[c]	—[c]	—[c]	—[c]	—[c]
006	Pre	0	0	5.4 (2.3)	1.5 (1.2)	2.4 (0.8)	1.1 (0.5)
	Post	78.4% (7.4)	1.6% (1.0)	26.6 (8.3)	2.0 (1.1)	4.4 (1.1)	4.4 (1.4)
007	Pre	0	0	1.9 (1.6)	11.1 (3.9)	10.1 (3.9)	2.9 (1.6)
	Post	75.9% (6.6)	0.5% (0.4)	3.9 (2.2)	15.3 (5.5)	16.9 (4.4)	4.7 (1.8)
010	Pre	0	0	2.0 (0.9)	13.3 (3.4)	13.1 (3.9)	2.9 (1.6)
	Post	—[c]	—[c]	—[c]	—[c]	—[c]	—[c]

[a]Number of positive cells per field (20×).
[b]% of positive cells.
[c]No tumor, fibrosis.

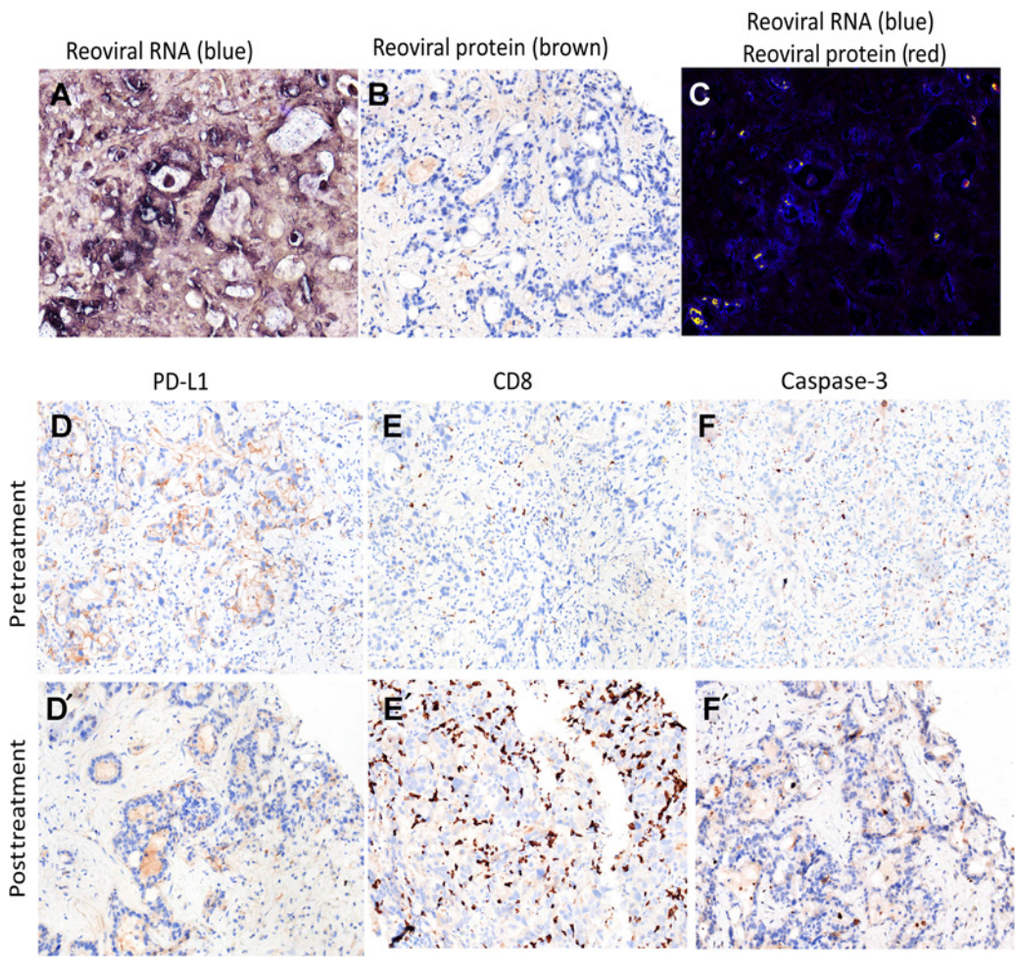

Figure 2.
Intravenously delivered pelareorep replicates in tumor tissues, promoting T-cell recruitment to the TME. Representative histologic analysis from patient No. 002. **A–C,** Micrographs for reoviral RNA in blue (**A**), reoviral capsid protein in brown (**B**), and a merged image with both viral RNA (blue) and protein (red; **C**). Analysis or pre- and post–PD-L1 (**D, D′**), CD8 (**E, E′**), and caspase-3 (**F, F′**) expression in the TME.

reaching statistical significance in patient No. 006. These data support the hypothesis that this treatment regime my help prime the TME as adjuncts for checkpoint blockade therapy.

Treatment-associated changes in the T-cell repertoire

Several studies have revealed that both local and systemic inflammation have an important role in cancer progression and response to immunotherapy. To assess the patient's ability to mount a systemic inflammatory response or immunological fitness for immunotherapy, we examined the neutrophil-to-lymphocyte ratio (NLR), which has been shown to correlate with patient outcomes in a variety of solid cancers, including PDAC (30–32). To perform this analysis, we separated patients into long-term survivors (LTS, OS > 6 months) and short-term survivors (STS, OS < 6 months). Consistent with previous reports, we found that a low NLR prior to the start of treatment (screening and C1D1) is associated better survival, where LTSs have a significantly lower NLR than STSs at screening, C1D1, and C2D1 (Supplementary Fig. S1A).

Given the potential roles for pelareorep and pembrolizumab to prime and activate T cells, we explored changes in the peripheral T-cell population by TCR immunosequencing. Specifically, we asked whether treatment would create new T-cell clones (via the release of novel neoantigen) or expand existing T-cell clones. TCR immunosequencing was performed with peripheral blood samples collected before treatment on C1D1, C1D8, and C2D1. To assess the T-cell repertoire, we calculated clonality, which quantifies the extent of mono- or oligoclonal dominance within a population. Clonality values range from 0 to 1, where larger values indicate a more clonal repertoire.

We found that there is a trend toward decreased peripheral clonality between C1D1 and C2D1, similarly, peripheral diversity, a measure of the number of unique rearrangements, which is often inverse but can be independent of clonality, increases during treatment (**Fig. 3A** and **B**). One patient in the study, No. 007 showed a large increase in clonality and decrease in diversity. Excluding patient No. 007, overall clonality significantly decreased ($P < 0.01$) while diversity significantly increased ($P = 0.019$). In addition to changes in clonality and diversity, we observed significant changes in T-cell repertoire turnover as measured by the Morisita index. The Morisita index calculates sample similarity, taking into account both overlap of clones and frequency. Values range from 0 (disparate) to 1 (identical). Normal variation over a month is approximately 0.9 to 0.95. The median Morisita index between C2D1 and C1D1 is 0.83 with three samples below 0.6, suggesting significant turnover within the peripheral T-cell population (**Fig. 3C**). Again, patient No. 007, who had a large increase in clonality, had a dramatically lower Morisita index of 0.25. At C2D1, differential abundance analysis reveals that clonal expansion in patient No. 007 is observed only from new clones and not the expansion of existing clones. Across patients, 86% of peripheral clonal expansion is observed from new clones (on the *y*-axis of differential abundance plots) rather than the expansion of existing clones (Supplementary Fig. S2). The number of T cells relative to the total nucleated cells (T-cell fraction) also increased during treatment with a significant increase at C1D8 ($P = 0.081$) and an overall, but not significant, increase at C2D1 ($P = 0.19$, **Fig. 3D**).

Correlative Cox regression analysis revealed that higher Simpson clonality is associated with improved PFS at C1D1 (**Fig. 3E**, HR = 0.1; $P = 0.030$) and C2D1 (**Fig. 3F**, HR = 0.080; $P = 0.073$). Similarly, higher Simpson clonality is also associated with better OS at C1D1 (**Fig. 3G**, HR = 0.104; $P = 0.014$) with a modest improvement in significance at C2D1 (**Fig. 3H**, HR = 0.023; $P = 0.007$). Similar values at C1D8 for both PFS and OS were also observed (Supplementary Fig. S3).

Importantly, all patients that achieved a PR or SD are characterized as having high peripheral clonality at C2D1. However, one patient with PD (No. 007) exhibited a significant increase in peripheral clonality at C2D1 and lived longer (7.1 months) than the median OS in this study. Thus, we examined the 6-month survival cutoff. LTSs have higher Simpson clonality at C1D1 (**Fig. 3I**, $P = 0.057$) and C2D1 (**Fig. 3J**, $P = 0.005$). Notably, there is an increasing separation or refinement in clonality between LTSs and STSs between C1D1 and C2D1 (**Fig. 3K**).

Comparison of clonal expansion at C1D8 and C2D1 indicated that C2D1 samples have significantly more clonal expansion where approximately 30% of expanded clones from C1D8 were also expanded at C2D1 (durable clones, **Fig. 3L**). Intriguingly, Spearman rho correlations show that the strongest trend with survival is seen with the expansion of early clones where both a high number of early clones and durable clones are associated with longer OS (**Fig. 3M** and **N**). Late clonal expansion (i.e., clones that expand after C1D8/pembrolizumab) does not appear to be associated with longer survival (**Fig. 3O**), indicating a potential priming effect with pelareorep and chemotherapy. However, we cannot rule out the disparate immunological effects of the different chemotherapy backbones or the role of chemotherapy alone in the creation of new clones.

Treatment-induced changes in peripheral blood chemokines and PBMC markers

The impact of immunotherapies is partly dependent on the ability to recruit different lymphocytes to the TME. $CD8^+$ cytotoxic T cells (CTL) are associated with prolonged survival and response to immunotherapies, in contrast, recruitment of regulatory T cells (Treg) is associated with resistance to immunotherapy and cancer progression. Since different immune cell types are attracted by separate sets of cytokines, we examined changes in the abundance CTL attracting cytokines (CXCL9/MIG, CXCL10/IP10, CXCL11/I-TAC) and Treg attracting chemokines (CCL22/MDC and CXCL12/SDF-1) from peripheral blood before treatment at C1D1, C1D8, and C2D1 with a Luminex assay. Notably, at C1D8 treatment with pelareorep and chemotherapy enhanced the abundance of CXCL9 ($P = 0.052$), with a statistically significant increase in CXCL10 ($P = 0.0003$) and CXCL11 ($P < 0.0001$) (Supplementary Fig. S4A–S4C). At C2D1, a statistically significant increase in abundance was observed for CXCL9 ($P < 0.0001$), CXCL10 ($P = 0.016$), and CXCL11 ($P = 0.001$). Examining Treg attracting chemokines revealed no significant changes in expression of both CCL22 and CXCL12 at C1D8 and C2D1 (Supplementary Fig. S4D and S4E).

When we analyzed immune gene expression in PBMCs, a significant change in expression of IFI27 and SIGLEC1 was observed over time (**Table 3A**). Subsequently, we evaluated differential expression of immune genes in patients with clinical benefit on study defined as CR, PR, or SD versus no clinical benefit (patients nonevaluable for radiographic response were removed from the analysis). Decreased expression (relative change <−1.5) of CD1b (C1D1), HLA-C, MAPK14 (C1D8), CD63, LY96, LTF, TXK, TNFSF13, IL25, C1QB (all at C2D1 time point) and increased expression (relative change > 1.5) of IL17F (C1D1), MAGEA4, CCL7 (both at C1D8), CSF1, ICOS, LILRA4, TICAM2 (all at C2D1 time point) was observed in patients with clinical benefit versus no clinical benefit (**Table 3B**, raw $P < 0.05$). Then, we analyzed immune gene expression in LTSs versus STSs. Changes in HLA-DRB4, TIGIT, TARP, SPA17, CXCR5, FCGR2A, HLA-C, KLRG1, CD83, and CD3D were associated with overall survival (unadjusted $P < 0.05$) but, after multiple adjustments, only decrease in expression of HLA-DRB4 was significantly associated with long-term survival (adjusted $P = 0.023$, all time points, **Table 3C**).

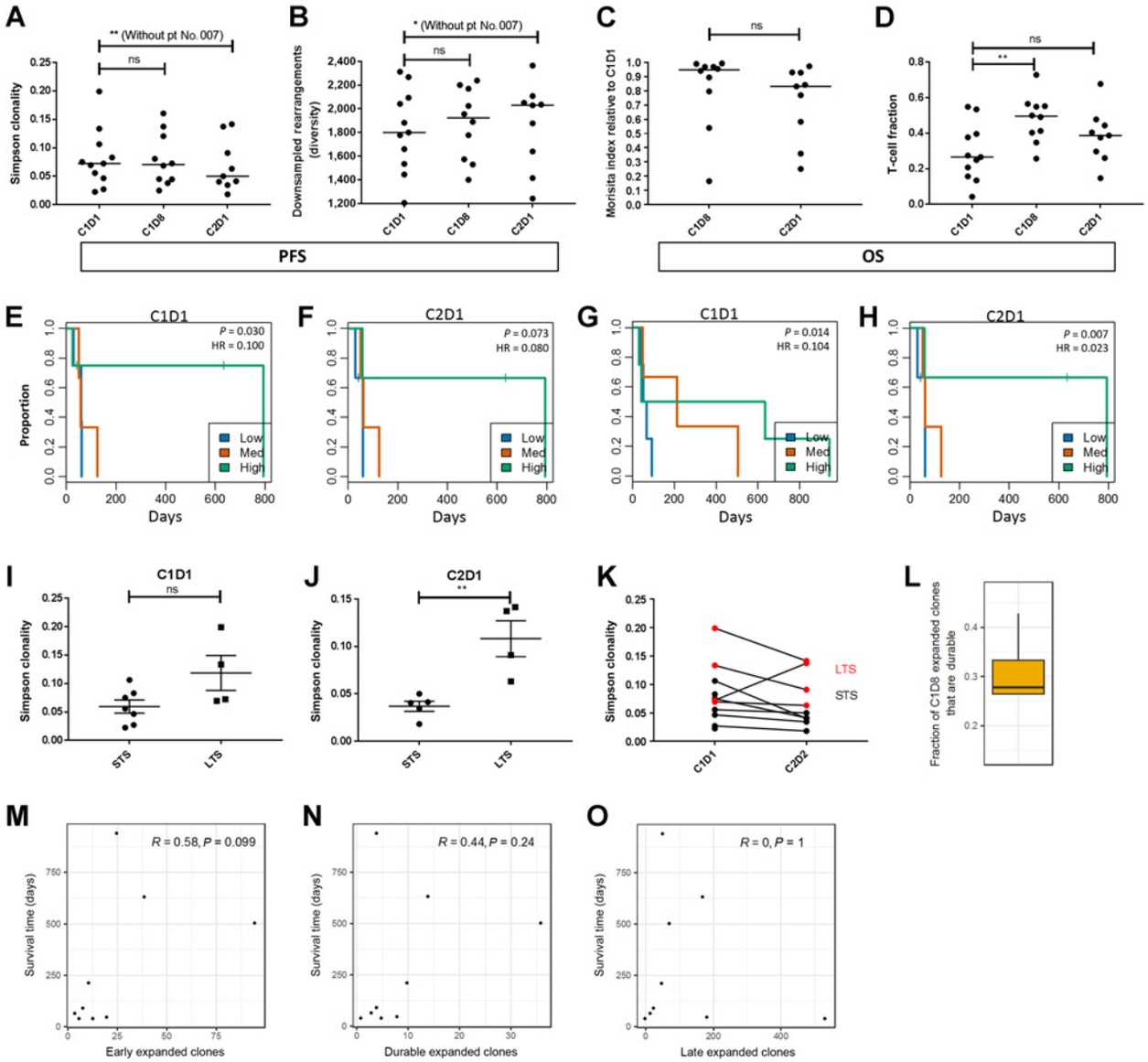

Figure 3.

Changes in T-cell clonality correlate with clinical outcome. **A–D,** Analysis of median Simpson clonality (**A**), median diversity (**B**; expressed as down sampled rearrangement), Morisita index between C1D1 and C2D1 (**C**), and T-cell fraction (**D**; the number of T cells relative to the total nucleated cells) during the first cycle of treatment at C1D1, C1D8, and C2D1 for each patient. Kaplan–Meier analysis examining progression-free survival by clonality at C1D1 (**E**) and C2D1 (**F**). *P* values and HR were determined using clonality as a continuous variable in the Cox regression, while high, medium, and low splits were used for visualization in Kaplan–Meier plot. Kaplan–Meier analysis examining overall survival by clonality at C1D1 (**G**) and C2D1 (**H**), statistics and plots were generated as in **E** and **F**. For both PFS and OS analyses, clonality was scaled to a unit of 0.1 for generating the HR. Patient level Simpson clonality values at C1D1 (**I**) and C2D1 (**J**) and the associated changes during the first cycle of treatment (**K**). The fraction of T-cell clones that expand at C1D8 and are durable at C2D1 (**L**). Spearman Rho correlations examining the relationship between overall survival and early expanded clones (**M**), durable expanded clones (**N**), and late expanded clones (**O**). ns, not significant; *, $P \leq 0.05$; **, $P \leq 0.01$.

As noted above, patient No. 007 survived significantly longer than other patients with PD with high T-cell clonality at C2D1 similar to patients with clinical benefit on study treatment. Thus, we sought to identify any unique changes in PBMC immune gene expression in this patient. After multiple adjustments, increased expression of CCL3L1 ($\log_2$ fold change 2.83, adjusted $P = 0.01$) differentiated patient No. 007. CCL3L1 (MIP-1α) is a ligand for chemokine receptors CCR1, CCR3, and CCR5 with chemotactic activities for lymphocytes and monocytes and also inhibitor for HIV infection (33, 34). Serum cytokine analysis also confirmed higher concentration of CCL3L1 (MIP-1α) in all time points for patient No. 007 (Supplementary Fig. S5).

Discussion

Building upon the preclinical and clinical evidence of immunomodulation with pelareorep in PDAC, we designed a phase Ib study of

Table 3. Gene expression analysis in PBMCs.

	C1D8	C2D1	Average expression	F	*P* value	Adjusted *P*
A. Immune gene expression over time						
IFI27	5.1	−0.89	7.65	20.56	<0.00001	0.001
SIGLEC1	3.43	1.03	7.42	13.27	<0.0001	0.025
CDK1	1.85	0.08	5.23	10.97	<0.001	0.061
MX1	1.88	0.81	10.56	9.34	<0.001	0.12
CD38	1.63	0.48	7.26	8.98	<0.001	0.12
B. Relative immune gene expression in patients with CR/PR/SD vs. PD (NE excluded)						
	C1D1	**C1D8**	**C2D1**	***P* value**		
CD1b	−1.66	—	—	0.03		
IL17F	1.8	—	—	0.01		
HLA-C	—	−2.06	—	0.04		
MAPK14	—	−1.83	—	0.04		
MAGEA4	—	1.55	—	0.05		
CCL7	—	1.69	—	0.02		
CD63	—	—	−2.13	0.03		
LY96	—	—	−1.93	0.02		
LTF	—	—	−1.89	0.02		
TXK	—	—	−1.72	0.02		
TNFSF13	—	—	−1.6	0.05		
IL25	—	—	−1.59	0.03		
C1QB	—	—	−1.51	0.04		
CSF1	—	—	1.73	0.03		
ICOS	—	—	2	0.04		
LILRA4	—	—	2.1	0.02		
TICAM2	—	—	2.28	0.03		
C. Immune gene expression in long- vs. short-term survivors (cutoff 6 months)						
	LogFC	**Average expression**	**t**	***P* value**	**Adjusted *P* value**	**B**
HLA-DRB4	−5.02	6.22	−4.84	<0.001	0.023	2.22
TIGIT	0.94	7.49	4.086165	<0.001	0.1	0.38
TARP	1.23	8.72	3.817007	<0.001	0.13	−0.27
SPA17	−1.39	4.31	−3.74	<0.001	0.13	−0.46
CXCR5	1.09	5.9	3.62	0.001	0.13	−0.77
FCGR2A	−1.2	11.09	−3.56	0.001	0.13	−0.88
HLA-C	−0.99	12.39	−3.52	0.001	0.13	−0.96
KLRG1	1.36	8.19	3.5	0.001	0.13	−1
CD83	0.75	6.02	3.34	0.002	0.17	−1.38
CD3D	0.89	9.56	3.15	0.003	0.25	−1.81

Abbreviation: NE, nonevaluable.

pelareorep in combination with an ICI and chemotherapy in patients with advanced, pre-treated PDAC. The treatment was well tolerated, and the most common toxicity was fever and chills (mostly grade 1 or 2). There were no immune-related AEs.

The efficacy results were encouraging with three evaluable patients showing long-term benefit from study treatment. Patient No. 001 achieved a PR lasting 17.4 months. This patient was previously treated with 5-FU–based chemoradiotherapy for locally advanced disease with SD as best response. Patient No. 005, initially diagnosed with locally advanced disease, had PR (near CR) with gemcitabine and nab-paclitaxel, but eventually progressed with metastatic disease to the liver. The patient subsequently enrolled in our study and attained SD lasting for approximately 4 months. Patient No. 010 was initially diagnosed with locally advanced disease and started treatment within a clinical trial incorporating chemotherapy, chemoradiotherapy and the PDAC vaccine Algenpantucel-L. This patient progressed with liver metastases within 3 months from last vaccine dose. Their disease stabilized on our study for 9.2 months. Additional immune priming for patients No. 001 and No. 010 from radiotherapy and or vaccine therapy cannot be definitively excluded but for patient No. 001, the fact that the response was first noted 6.5 months after beginning study therapy makes this highly unlikely. To explore the possibility of hyperprogression in nonresponding patients, we examined known physiologic features associated with hyperprogression such as baseline differential abundance in albumin, LDH, lymphocyte/neutrophil/platelets ratios as well as the baseline sum diameter of target lesions. As shown in Supplementary Fig. S1A, nonresponding patients/STSs have a higher lymphocyte/neutrophil ratio and higher lymphocyte/neutrophil × platelets ratios at screening (Supplementary Fig. S1B). Nonresponding patients/STSs also have lower levels of albumin, although this was not statistically significant (Supplementary Fig. S1C). No differences were observed between responders and nonresponders with respect to baseline LDH levels and baseline tumor volume (Supplementary Fig. S1D and S1E).

The extent of viral replication assessed by an examination of reoviral dsRNA and capsid protein is consistent with reports from previous studies, where dsRNA ranges from 20% to 100% of tumor cells, while the presence of capsid protein/lytic replication is in the range of 0% to 20% (17, 18, 35). In this study, posttreatment biopsies did not contain normal pancreatic tissue; however, previous studies have

demonstrated that viral proliferation and immunologic effects are specific to tumor cells and not adjacent normal tissue (17, 18). The time points examined in this study and the degree of proliferating cancer cells may also be a contributing factor, as Samson and colleagues found that genomic (dsRNA) and lytic (capsid protein) viral replication is associated with cell proliferation assessed by Ki67 (17). Furthermore, induction of necroptosis (an alternative form of cell death) from reovirus infection requires, in addition to IFN production, active dsRNA synthesis that was present in the evaluable on-treatment specimens (36). A negative effect of pembrolizumab on viral replication cannot be excluded (37) but complete viral replication in the tumor may not be a prerequisite for induction of antitumor immune response, as reovirus-activated dendritic cells can activate NK cells and CTLs against uninfected tumor cells (16). Increase in intertumoral $CD8^+$ T cells was noted in this study; however, the small sample size precludes any meaningful association with capsid protein expression. In addition, we noted increased expression of LILRA4 and ICOS after pembrolizumab administration in patients who derived clinical benefit on-study. LILRA4 expression characterizes plasmacytoid dendritic cells that are the major source of type I IFN production in response to reovirus infection and serves as a mechanism to counteract excessive IFN production from these cells (38, 39). Furthermore, ICOS has been implicated to the induction IFNγ in response to reovirus infection (40).

In this study, we attempted a comprehensive characterization of changes in systemic immunity with pelareorep and sought to determine how ICIs can modify these effects. However, we are precluded from an in-depth characterization of the disparate immunological effects of the different chemotherapy backbones. To that end, we decided to sequence pelareorep and pembrolizumab administration by dosing pelareorep first. Three time points for peripheral blood collection were selected to assess the immune system at baseline, after pelareorep priming (C1D8) and finally after combined therapy (C2D1). This strategy allowed us to characterize emerging and expanding T-cell clones from each constituent of the combination strategy. We found that, although clonal expansion was more pronounced after pembrolizumab, it was the early clonal expansion achieved with pelareorep priming as well as the durable clonal expansion that appeared to be associated with improved long-term outcomes. To our knowledge, these results are unique in terms of identifying the significance of the immune priming effect of immune adjuncts in PDAC and the maintenance of this effect by ICIs.

Similar to our study, research by Hopkins and colleagues found that patients with PDAC treated with nivolumab and a *Listeria monocytogenes* bacteria expressing mesothelin experience an increase in clonal diversity in peripheral T cells after thee cycles of treatment (41). Importantly, Hopkins and colleagues also found that LTSs (OS > 6 months) have higher levels of peripheral T-cell clonality posttreatment relative to STSs (OS < 6 months). Thus, peripheral T-cell clonality may by an important biomarker for checkpoint blockade therapy administered in combination with immune priming agents such as oncolytic viruses or cancer vaccines.

Circulating (plasma) chemokine analysis in our study revealed increases in the abundance of multiple IFN-inducible chemokines known to recruit CTL attractants (CXCL9/MIG, CXCL10/IP10, CXCL11/I-TAC) during the first treatment cycle. This is consistent with previous reports demonstrating pelareorep-mediated activation of IFN signaling and downstream effector proteins such as CXCL9/10/11. However, in this study, we only observed a small, but not statistically significant, increase in IFNγ and IFNβ expression (Supplementary Fig. S6). Previous studies have indicated that IFN expression may be under tight temporal regulation and peak approximately 48 hours after pelareorep infusion (20); thus, analysis at C1D8 may not be suitable time point to fully interrogate the IFN pathway. However, we did observe an increased expression of IFI27 in PBMCs that is involved in type I IFN-induced apoptosis (42). Intriguingly, there were no differences in the abundance of cytokines known to recruit Tregs (CCL22/MDC, CXCL12/SDF-1). Furthermore, on-treatment IL25 expression in PBMCs decreased in patients who had controlled disease. On the contrary, Noonan and colleagues observed increase in SDF-1 and Tregs by flow cytometry (43). This may be related to the different chemotherapy backbones utilized, with gemcitabine having a favorable immunomodulatory effect in combination with pelareorep (7). Future research will also need to examine whether this is due to the differential activation of dsRNA signaling pathways, such as TLR3, versus helicases (RIG-I/MDA-5), which can differentially activate CTL and Treg attractants (29). So far, reovirus appears to decrease the immunosuppressive activity of myeloid-derived suppressor cells through a TLR3-dependent mechanism (44). Interestingly, expression of TICAM2 (a TLR4 pathway adaptor protein, reviewed in ref. 45) was increased after pembrolizumab administration in patients who derived benefit on-study, which provides new insights into the potential cross-talk between the TLR4 and PD-1/PD-L1 pathways in viral infections (46).

Finally, patient No. 007 followed a distinct immune pattern as compared with the other patients. Although conclusions are limited with one patient out of 11, patient No. 007's results provide a compelling starting point for future hypothesis testing. As noted above, this patient had significant increase in T-cell clonality at C2D1, similar to patients with clinical benefit though the OS was significantly longer than the rest of the patients with progressive or nonevaluable disease. Patient No. 007 was previously treated with gemcitabine and nab-paclitaxel with PD as best response and also progressed within 3 months on study therapy. CCL3L1 expression in PBMCs and serum concentration was higher for patient No. 007 at all time points. Although reovirus has been shown to be able to induce CCL3L1 production in infected melanoma and breast carcinoma cells *in vitro* (11, 47), patient No. 007 had elevated serum levels at baseline with no significant change at C1D8 or C2D1. CCR5 is a coreceptor for HIV and its ligand CCL3L1 is an inhibitor of HIV infection (33, 34). It is likely that high CCL3L1 can be protective against reovirus infection as CCR5 is associated with antireovirus immune response (48). Intriguingly, viral capsid expression in patient No. 007 was also the lowest among all patients with evaluable posttreatment tumor biopsy. Further studies should focus on the role of CCR5 and its ligands as a negative predictive biomarker for pelareorep therapy or other oncolytic virotherapy.

Conclusion

Pelareorep in combination with chemotherapy and pembrolizumab in patients with advanced, pretreated PDAC was well-tolerated and showed prolonged efficacy in three patients. Viral immunomodulation was evident, with early and durable clones associated with long-term outcomes, but given our small sample size, this should be examined as a dynamic predictive biomarker in future studies with oncolytic viruses. A follow-up phase II study with pelareorep and pembrolizumab, without chemotherapy, in second-line pancreatic cancer is underway (NCT03723915).

Disclosure of Potential Conflicts of Interest

D. Mahalingam is an employee/paid consultant for EMD Serono, reports receiving commercial research grants from Oncolytics and Merck, reports receiving speakers bureau honoraria from Amgen, EISAI, Genentech, and Bayer, and reports receiving

other remuneration from Blake Jones Law Firm. G. Wilkinson is an employee/paid consultant for and holds ownership interest (including patents) in Oncolytics Biotech Inc. P. Fields is an employee/paid consultant for Adaptive Biotechnologies. P. Raber is an employee/paid consultant for and holds ownership interest (including patents) in Adaptive Biotechnologies Corp. K. Cheetham is an employee/paid consultant for Oncolytic Biotech Inc. M. Coffey is an employee/paid consultant for and holds ownership interest (including patents) in Oncolytic Biotech Inc. G. Nuovo is an employee/paid consultant for Oncolytics. S.P. Arora reports receiving speakers bureau honoraria from Exelixis and Bayer. C. Fountzilas is an advisory board member/unpaid consultant for AstraZeneca. No potential conflicts of interest were disclosed by the other authors.

Authors' Contributions

Conception and design: D. Mahalingam, M. Coffey, P. Kalinski, C. Fountzilas
Development of methodology: D. Mahalingam, G.A. Wilkinson, G. Nuovo, C. Fountzilas
Acquisition of data (provided animals, acquired and managed patients, provided facilities, etc.): D. Mahalingam, G.A. Wilkinson, J.L. Moseley, G. Nuovo, S.P. Arora, C. Fountzilas
Analysis and interpretation of data (e.g., statistical analysis, biostatistics, computational analysis): D. Mahalingam, G.A. Wilkinson, K.H. Eng, P. Fields, P. Raber, G. Nuovo, P. Kalinski, B. Zhang, S.P. Arora, C. Fountzilas
Writing, review, and/or revision of the manuscript: D. Mahalingam, G.A. Wilkinson, K.H. Eng, P. Fields, P. Raber, K. Cheetham, M. Coffey, G. Nuovo, P. Kalinski, B. Zhang, S.P. Arora, C. Fountzilas
Administrative, technical, or material support (i.e., reporting or organizing data, constructing databases): G.A. Wilkinson, K.H. Eng, J.L. Moseley, K. Cheetham, S.P. Arora
Study supervision: D. Mahalingam, S.P. Arora
Other (contributed to the design of the correlative studies and the current article): P. Kalinski

Acknowledgments

Oncolytics Biotech Inc. provided pelareorep and partial funding. The correlative studies were partially funded by a grant provided by the Roswell Park Alliance Foundation. C. Fountzilas was a recipient of a Cancer Research Training Award (RP 140105) funded by the Cancer Prevention & Research Institute of Texas. This work was supported by NCI grant P30CA016056 involving the use of Roswell Park Comprehensive Cancer Center's Genomic Shared Resource. Luminex cytokine analysis services were provided by the Flow and Image Cytometry Core facility at the Roswell Park Comprehensive Cancer Center, which is supported in part by the NCI Cancer Center Support Grant P30CA016056. SPA: NIH CA054174, NIA AG044271.

The costs of publication of this article were defrayed in part by the payment of page charges. This article must therefore be hereby marked *advertisement* in accordance with 18 U.S.C. Section 1734 solely to indicate this fact.

Received June 24, 2019; revised August 16, 2019; accepted October 9, 2019; published first November 6, 2019.

References

1. Siegel RL, Miller KD, Jemal A. Cancer statistics, 2019. CA Cancer J Clin 2019;69:7–34.
2. Wolfgang CL, Herman JM, Laheru DA, Klein AP, Erdek MA, Fishman EK, et al. Recent progress in pancreatic cancer. CA Cancer J Clin 2013;63:318–48.
3. Jemal A, Siegel R, Ward E, Hao Y, Xu J, Thun MJ, et al. Cancer statistics, 2009. CA Cancer J Clin 2009;59:225–49.
4. Conroy T, Desseigne F, Ychou M, Bouché O, Guimbaud R, Bécouarn Y, et al. FOLFIRINOX versus gemcitabine for metastatic pancreatic cancer. N Engl J Med 2011;364:1817–25.
5. Von Hoff DD, Ervin T, Arena FP, Chiorean EG, Infante J, Moore M, et al. Increased survival in pancreatic cancer with nab-paclitaxel plus gemcitabine. N Engl J Med 2013;369:1691–703.
6. Fountzilas C, Patel S, Mahalingam D. Review: Oncolytic virotherapy, updates and future directions. Oncotarget 2017;8:102617–39.
7. Gujar SA, Clements D, Dielschneider R, Helson E, Marcato P, Lee PW. Gemcitabine enhances the efficacy of reovirus-based oncotherapy through anti-tumour immunological mechanisms. Br J Cancer 2014;110:83–93.
8. Lolkema MP, Arkenau HT, Harrington K, Roxburgh P, Morrison R, Roulstone V, et al. A phase I study of the combination of intravenous reovirus type 3 Dearing and gemcitabine in patients with advanced cancer. Clin Cancer Res 2011;17:581–8.
9. Mahalingam D, Goel S, Aparo S, Patel Arora S, Noronha N, Tran H, et al. A phase II study of pelareorep (REOLYSIN((R))) in combination with gemcitabine for patients with advanced pancreatic adenocarcinoma. Cancers 2018;10:pii:E160.
10. Ilett E, Kottke T, Thompson J, Rajani K, Zaidi S, Evgin L, et al. Prime-boost using separate oncolytic viruses in combination with checkpoint blockade improves anti-tumour therapy. Gene Ther 2017;24:21–30.
11. Mostafa AA, Meyers DE, Thirukkumaran CM, Liu PJ, Gratton K, Spurrell J, et al. Oncolytic reovirus and immune checkpoint inhibition as a novel immunotherapeutic strategy for breast cancer. Cancers 2018;10:pii:E205.
12. Rajani K, Parrish C, Shim K, Ilett L, Thompson J, Kottke T, et al. Combination therapy of reovirus and PD-1 blockade effectively establishes tumor control via innate and adaptive immune responses. Cancer Res 2015;75:Abstract 1360.
13. Gujar S, Pol JG, Kim Y, Lee PW, Kroemer G. Antitumor benefits of antiviral immunity: an underappreciated aspect of oncolytic virotherapies. Trends Immunol 2018;39:209–21.
14. Steele L, Errington F, Prestwich R, Ilett E, Harrington K, Pandha H, et al. Pro-inflammatory cytokine/chemokine production by reovirus treated melanoma cells is PKR/NF-kappaB mediated and supports innate and adaptive anti-tumour immune priming. Mol Cancer 2011;10:20.
15. Gujar SA, Marcato P, Pan D, Lee PW. Reovirus virotherapy overrides tumor antigen presentation evasion and promotes protective antitumor immunity. Mol Cancer Ther 2010;9:2924–33.
16. Errington F, Steele L, Prestwich R, Harrington KJ, Pandha HS, Vidal L, et al. Reovirus activates human dendritic cells to promote innate antitumor immunity. J Immunol 2008;180:6018–26.
17. Samson A, Scott KJ, Taggart D, West EJ, Wilson E, Nuovo GJ, et al. Intravenous delivery of oncolytic reovirus to brain tumor patients immunologically primes for subsequent checkpoint blockade. Sci Transl Med 2018;10:pii:eaam7577.
18. Adair RA, Roulstone V, Scott KJ, Morgan R, Nuovo GJ, Fuller M, et al. Cell carriage, delivery, and selective replication of an oncolytic virus in tumor in patients. Sci Transl Med 2012;4:138ra77.
19. Adair RA, Scott KJ, Fraser S, Errington-Mais F, Pandha H, Coffey M, et al. Cytotoxic and immune-mediated killing of human colorectal cancer by reovirus-loaded blood and liver mononuclear cells. Int J Cancer 2013;132:2327–38.
20. El-Sherbiny YM, Holmes TD, Wetherill LF, Black EV, Wilson EB, Phillips SL, et al. Controlled infection with a therapeutic virus defines the activation kinetics of human natural killer cells *in vivo*. Clin Exp Immunol 2015;180:98–107.
21. Keir ME, Butte MJ, Freeman GJ, Sharpe AH. PD-1 and its ligands in tolerance and immunity. Annu Rev Immunol 2008;26:677–704.
22. Eisenhauer EA, Therasse P, Bogaerts J, Schwartz LH, Sargent D, Ford R, et al. New response evaluation criteria in solid tumours: revised RECIST guideline (version 1.1). Eur J Cancer 2009;45:228–47.
23. Wolchok JD, Hoos A, O'Day S, Weber JS, Hamid O, Lebbé C, et al. Guidelines for the evaluation of immune therapy activity in solid tumors: immune-related response criteria. Clin Cancer Res 2009;15:7412–20.
24. Nuovo GJ. In situ detection of microRNAs in paraffin embedded, formalin fixed tissues and the co-localization of their putative targets. Methods 2010;52:307–15.
25. Carlson CS, Emerson RO, Sherwood AM, Desmarais C, Chung MW, Parsons JM, et al. Using synthetic templates to design an unbiased multiplex PCR assay. Nat Commun 2013;4:2680.
26. DeWitt WS, Emerson RO, Lindau P, Vignali M, Snyder TM, Desmarais C, et al. Dynamics of the cytotoxic T cell response to a model of acute viral infection. J Virol 2015;89:4517–26.
27. Ritchie ME, Phipson B, Wu D, Hu Y, Law CW, Shi W, et al. limma powers differential expression analyses for RNA-sequencing and microarray studies. Nucleic Acids Res 2015;43:e47.
28. Benjamini Y, Hochberg Y. Controlling the false discovery rate: a practical and powerful approach to multiple testing. J Royal Stat Soc: Ser B Methodol 1995;57:289–300.

29. Theodoraki MN, Yerneni S, Sarkar SN, Orr B, Muthuswamy R, Voyten J, et al. Helicase-driven activation of NFkappaB-COX2 pathway mediates the immunosuppressive component of dsRNA-driven inflammation in the human tumor microenvironment. Cancer Res 2018;78:4292–302.
30. Gao Y, Wang WJ, Zhi Q, Shen M, Jiang M, Bian X, et al. Neutrophil/lymphocyte ratio is a more sensitive systemic inflammatory response biomarker than platelet/lymphocyte ratio in the prognosis evaluation of unresectable pancreatic cancer. Oncotarget 2017;8:88835–44.
31. Sacdalan DB, Lucero JA, Sacdalan DL. Prognostic utility of baseline neutrophil-to-lymphocyte ratio in patients receiving immune checkpoint inhibitors: a review and meta-analysis. Onco Targets Ther 2018;11:955–65.
32. Zhou Y, Wei Q, Fan J, Cheng S, Ding W, Hua Z. Prognostic role of the neutrophil-to-lymphocyte ratio in pancreatic cancer: a meta-analysis containing 8252 patients. Clin Chim Acta 2018;479:181–9.
33. Proost P, Menten P, Struyf S, Schutyser E, De Meester I, Van Damme J. Cleavage by CD26/dipeptidyl peptidase IV converts the chemokine LD78beta into a most efficient monocyte attractant and CCR1 agonist. Blood 2000;96:1674–80.
34. Struyf S, Menten P, Lenaerts JP, Put W, D'Haese A, De Clercq E, et al. Diverging binding capacities of natural LD78beta isoforms of macrophage inflammatory protein-1alpha to the CC chemokine receptors 1, 3 and 5 affect their anti-HIV-1 activity and chemotactic potencies for neutrophils and eosinophils. Eur J Immunol 2001;31:2170–8.
35. Sborov DW, Nuovo GJ, Stiff A, Mace T, Lesinski GB, Benson DM Jr, et al. A phase I trial of single-agent reolysin in patients with relapsed multiple myeloma. Clin Cancer Res 2014;20:5946–55.
36. Berger AK, Hiller BE, Thete D, Snyder AJ, Perez E Jr, Upton JW, et al. Viral RNA at two stages of reovirus infection is required for the induction of necroptosis. J Virol 2017;91:pii:e02404-16.
37. Cortese I, Muranski P, Enose-Akahata Y, Ha SK, Smith B, Monaco MC, et al. Pembrolizumab treatment for progressive multifocal leukoencephalopathy. N Engl J Med 2019;380:1597–605.
38. Johansson C, Wetzel JD, He J, Mikacenic C, Dermody TS, Kelsall BL. Type I interferons produced by hematopoietic cells protect mice against lethal infection by mammalian reovirus. J Exp Med 2007;204:1349–58.
39. Cao W, Bover L, Cho M, Wen X, Hanabuchi S, Bao M, et al. Regulation of TLR7/9 responses in plasmacytoid dendritic cells by BST2 and ILT7 receptor interaction. J Exp Med 2009;206:1603–14.
40. Montufar-Solis D, Garza T, Teng BBKlein JR Upregulation of ICOS on CD43+ CD4+ murine small intestinal intraepithelial lymphocytes during acute reovirus infection. Biochem Biophys Res Commun 2006;342:782–90.
41. Hopkins AC, Yarchoan M, Durham JN, Yusko EC, Rytlewski JA, Robins HS, et al. T cell receptor repertoire features associated with survival in immunotherapy-treated pancreatic ductal adenocarcinoma. JCI Insight 2018;3:pii:122092.
42. Rosebeck S, Leaman DW. Mitochondrial localization and pro-apoptotic effects of the interferon-inducible protein ISG12a. Apoptosis 2008;13:562–72.
43. Noonan AM, Farren MR, Geyer SM, Huang Y, Tahiri S, Ahn D, et al. Randomized phase 2 trial of the oncolytic virus pelareorep (reolysin) in upfront treatment of metastatic pancreatic adenocarcinoma. Mol Ther 2016;24:1150–8.
44. Katayama Y, Tachibana M, Kurisu N, Oya Y, Terasawa Y, Goda H, et al. Oncolytic reovirus inhibits immunosuppressive activity of myeloid-derived suppressor cells in a TLR3-dependent manner. J Immunol 2018;200:2987–99.
45. O'Neill LA, Bowie AG. The family of five: TIR-domain-containing adaptors in Toll-like receptor signalling. Nat Rev Immunol 2007;7:353–64.
46. Wang Y, Chung YR, Eitzinger S, Palacio N, Gregory S, Bhattacharyya M, et al. TLR4 signaling improves PD-1 blockade therapy during chronic viral infection. PLoS Pathog 2019;15:e1007583.
47. Errington F, White CL, Twigger KR, Rose A, Scott K, Steele L, et al. Inflammatory tumour cell killing by oncolytic reovirus for the treatment of melanoma. Gene Ther 2008;15:1257–70.
48. McAlpine SM, Issekutz TB, Marshall JS. Virus stimulation of human mast cells results in the recruitment of CD56(+) T cells by a mechanism dependent on CCR5 ligands. FASEB J 2012;26:1280–9.